communications earth & environment

Article

A Nature Portfolio journal

https://doi.org/10.1038/s43247-025-02317-x

Widespread sea surface salinification induced by tropical cyclones over the Changjiang River Plume

Shoude Guan [1,2,3,4,11] ✉, Mengya Huang [1,11], I-I Lin[5], Hui Wu [6] ✉, Yaoting Lin[6], Ziyi Wu[1], Yihan Zhang[1], Fei-Fei Jin [7], Weili Wang[8], Xin Hong[9], Cheng Li[10], Zhenmin Liu[10], Xiaopei Lin [1,2,3,4], Wei Zhao [1,2,3,4] ✉ & Jiwei Tian [1,2,3,4]

Riverine plumes greatly shape ocean environments and ecosystems. The Changjiang River plume, widely spreading in the Yellow and East China Seas in summer, induces extremely low surface salinity and threatens local aquaculture and fisheries. Passage of tropical cyclones potentially increases surface salinity by stirring upper oceans, yet the extent of cyclones' effects on the Changjiang River Plume extension and its mechanisms remains less explored. Here, combining satellite and in-situ observations with numerical experiments, we reveal a widespread surface salinification induced by Lekima (2019), with the maximum salinification reaching 6.5 psu and an 83% Changjiang River Plume contraction. Tropical cyclone-induced vertical mixing contributes to this dramatic salinification, while horizontal advection can either contribute to or offset the salinification, depending on specific locations. Further examination of surface salinity during 2015–2022 suggests that tropical cyclones can effectively restrict the Changjiang River Plume extension, potentially shielding fishing and aquaculture industries from low-salinity-related disasters.

Tropical cyclones (TCs), also known as typhoons or hurricanes, are among the deadliest natural hazards on earth and cause devastating damage to lives and property in coastal regions annually[1]. With strong wind forcing, TC-induced strong mixing and upwelling act to bring cold, salty, and nutrient-rich subsurface water into the surface layer, triggering a cold, salty wake, and stimulating phytoplankton blooms[2–9]. These profound responses can not only have feedback on the subsequent TC intensification[1,10,11] but also influence the global climate and primary production[12].

TC-induced thermal response, usually manifested as a 1–10 °C sea surface temperature (SST) decrease, has been fairly well examined in recent decades based on in situ and satellite observations[13–20]. In contrast, the haline response to TCs is relatively less explored due to the sparsity of sea surface salinity (SSS) observations. Based on in-situ observations from buoys or Argos occasionally encountering TCs, few studies reported that SSS increases induced by individual TCs could be over 1 psu[21–27]. Since 2009, SSS measurements from L-band microwave radiometers on board the Soil Moisture and Ocean Salinity (SMOS), Aquarius, and Soil Moisture Active Passive (SMAP) missions have been successively available, enabling the mapping of the spatiotemporal variability of TC-induced SSS changes more precisely[5,28–31]. For example, using Aquarius and SMOS observations, the research[31] reported a 1–2 psu SSS increase when Hurricane Katia (2011) passed over the Amazon-Orinoco River plume (AORP). Combining 10-year satellite observations, four regions are identified with the most striking SSS increases due to the presence of barrier layers, i.e., the AORP, Bay of Bengal, Mississippi, and Changjiang (Yangtze) River plume (CRP), all with large freshwater input from river discharge or local rainfall[5]. It has been demonstrated that the strong haline stratification of the barrier layer over the AORP and CRP helps to suppress vertical mixing and reduce SST cooling under TCs, thus favoring TC intensification[10,20,32].

[1]Frontier Science Center for Deep Ocean Multispheres and Earth System (FDOMES) and Physical Oceanography Laboratory/Academy of Future Ocean, Ocean University of China, Qingdao, China. [2]Key Laboratory of Ocean Observation and Information of Hainan Province, Sanya Oceanographic Institution, Sanya, China. [3]Sanya Oceanographic Laboratory, Sanya, China. [4]Laoshan Laboratory, Qingdao, China. [5]Department of Atmospheric Sciences, National Taiwan University, Taipei, Taiwan. [6]State Key Laboratory of Estuarine and Coastal Research, and School of Marine Sciences, East China Normal University, Shanghai, China. [7]Department of Atmospheric Sciences, SOEST, University of Hawaii at Manoa, Honolulu, Hawaii, USA. [8]Hainan Institute of Zhejiang University, Sanya, China. [9]Yantai Ocean Environment Monitoring Center Station of State Oceanic Administration, Yantai, China. [10]National Marine Data and Information Service, Tianjin, China. [11]These authors contributed equally: Shoude Guan, Mengya Huang. ✉e-mail: guanshoude@ouc.edu.cn; hwu@sklec.ecnu.edu.cn; weizhao@ouc.edu.cn

The CRP, located in the shallow shelf of the Yellow and East China Seas (YECS), with an average water depth of about 60 m, is formed by mixing Changjiang discharged fresh water with ambient saline water[33]. In boreal summer, due to increasing river discharge and summer monsoon winds[34], the low-salinity CRP widely extends within the YECS and can reach the vicinity of Jeju Island[35,36]. This extension of extremely low-salinity water can cause severe fishery damage[37,38] since the YECS is one of the most favorable fishing grounds in the world[39]. Meanwhile, approximately three TCs pass over the YECS annually in the summertime, which potentially induces an SSS increase and thus affects the CRP extension[40–44]. In contrast to the extensive studies on the haline response to TCs in the AORP, Mississippi, and the Bay of Bengal[28,29,31,45], the impact of TCs on the SSS evolution in the YECS has received much less attention. Despite previous studies demonstrating that TCs increased the CRP SSS via entraining saltier subsurface water to the fresher surface[40–43], a detailed examination of the extent of TC-induced SSS increases in the CRP and the underlying mechanisms is still lacking.

In August 2019, Super Typhoon Lekima, the second-costliest TC in Chinese history, passed over and influenced the CRP for three days when moving northward along the China mainland coast. Hereby combining satellite, in situ observations, and model experiments, we characterize the SSS response in the CRP to Lekima and explore the underlying mechanisms. We find that Super Typhoon Lekima caused a widespread increase in SSS across the YECS, with the most notable increase occurring within the CRP. This led to a dramatic 83% reduction in the low-SSS CRP area, which previously extended widely across the YECS, confined to the vicinity of the Changjiang estuary. This dramatic increase in SSS is mainly due to the TC-induced vertical mixing and horizontal advection. Our study highlights TCs' crucial role in reducing extremely low salinity conditions in the YECS, thereby offering potential protection to the region's local fish industries from the adverse effects of diluted seawater.

Results

Widespread sea surface salinification induced by Lekima

We characterize CRP SSS and SST response to Super Typhoon Lekima, using satellite observations, which are validated by buoy data (see "Super Typhoon Lekima" and "Satellite data" in Methods). Figure 1 illustrates pre-, post-TC SSS, and SST and their changes induced by Lekima. Before the passage of Lekima, low-SSS CRP prevailed in the YECS and extended toward Jeju Island in the shape of a tongue (Fig. 1a), typically forming a barrier layer[20,46,47]. Areas encompassed by 28 and 30 psu isohalines reach $5.68 \times 10^4\,km^2$ and $2.06 \times 10^5\,km^2$, respectively (Supplementary Fig. 1). A northward-extending warm tongue is observed within this low-salinity region, as indicated by the 28 °C isotherm. The co-occurrence of the low-SSS CRP extension and warm tongue is likely because the low-SSS-related barrier layers can restrain the downward heat transport and result in surface warming[29,48].

After the Lekima passage, a widespread increase in SSS was detected by satellite observations (Fig. 1b, c). The low-SSS CRP region, previously widely extending in the YECS, contracted to the vicinity of the Changjiang estuary. The area with SSS smaller than 28 psu decreased to approximately $9.85 \times 10^3\,km^2$, indicating an 83% CRP contraction. The CRP occupies a larger SSS increase than surrounding areas, with the maximum SSS increase

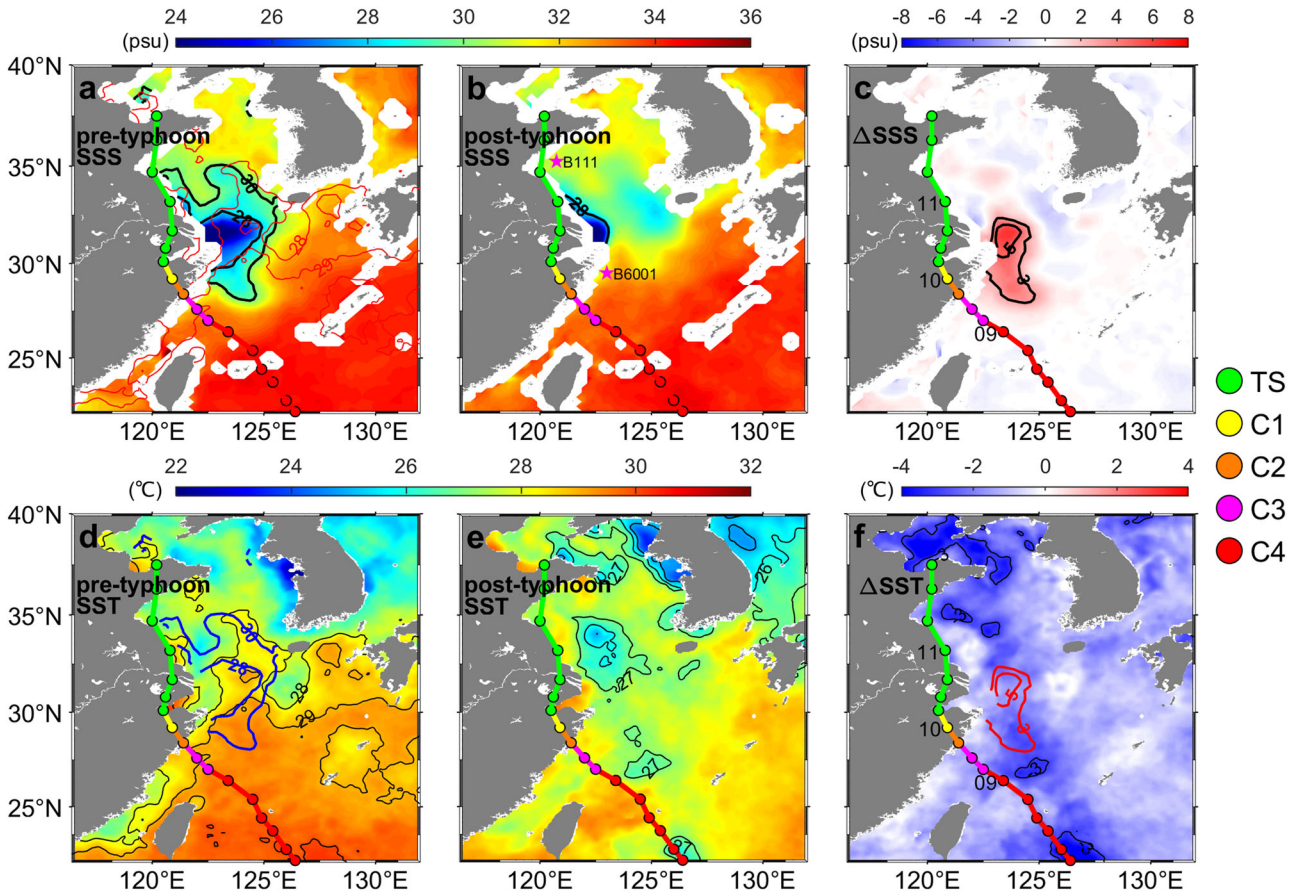

Fig. 1 | Sea surface salinity (SSS) and temperature (SST) responses to Super Typhoon Lekima. a Spatial pattern of SSS before Lekima passage.Colored-solid line with dots denotes the track of Lekima; 28 and 30 psu isohalines and 28 and 29 °C isotherms are contoured. **b** Same as (**a**), but after Lekima passage. Magenta stars denote the locations of buoys B111 and B6001, which are located in the Yellow Sea and the East China Sea, respectively. **c** Lekima-induced SSS changes. +3 and +5 psu isohalines are contoured. **d**–**f** Same as (**a**–**c**), but for the spatial pattern of SST. Abbreviations: TS tropical storm, C1 Category 1, C2 Category 2, C3 Category 3, C4 Category 4.

reaching 6.5 psu. The areas encompassed by +3 and +5 psu isohalines are 6.87×10^4 km^2 and 1.34×10^4 km^2, respectively.

Given potential uncertainties in satellite observations near coastlines due to radio-frequency interference[49], the accuracy of the satellite-observed SSS increases against in-situ buoy B111 observations is evaluated (Supplementary Fig. 2). The correlation coefficient between satellite and buoy observations reaches 0.81, statistically significant above the 99% confidence level. Bias and root-mean-square error (RMSE) of satellite SSS against buoy observations are only 0.09 psu and 0.16 psu, respectively. These results indicate a good reliability of satellite observations in capturing the SSS changes induced by TCs. In contrast to the pronounced SSS increase, Lekima-induced SST cooling within the CRP was relatively weak compared to the surrounding regions in the YECS (Fig. 1d–f). Within the CRP, the maximum SST cooling is around −2.9 °C, whereas the maximum SST cooling over the surrounding area reached up to −5.0 °C. The haline stratification fostered by the low-salinity surface water and underlying barrier layer in the CRP tends to enhance salinification while mitigating cooling effects. This leads to a saltier and warmer response to TCs in the CRP compared to surrounding regions[5,44,46,48].

Mechanisms of Lekima-induced surface salinification

Before the passage of Lekima on August 5, east winds smaller than 5 m s^{-1} prevailed in the YECS (Supplementary Fig. 3a). However, when Lekima passed over the CRP on August 9, the wind direction shifted to the southeast, with speeds increasing to over 17 m s^{-1} (Supplementary Fig. 3b), before shifting to south winds after the Lekima passage (Supplementary Fig. 3c). The onshore southeasterly winds during Lekima passage can drive horizontal advection of the low-salinity CRP and surrounding salty waters northwestward, resulting in the encroachment of salty waters into the region originally occupied by the low-salinity CRP waters. Thus, the horizontal advection potentially contributes to the observed SSS increase.

Available radar sea surface current observations in the CRP during Lekima passage, in combination with satellite SSS, allow us to explore the effects of horizontal advection on SSS increase within the radar-covered region (see "Radar observations" in Methods). On August 5, surface currents were relatively weak at about 0.08 m s^{-1} (Fig. 2a). On August 9, under the influence of Lekima's strong winds, the currents increased to approximately 0.62 m s^{-1} and flowed from high- to low-SSS water (Fig. 2b). Correspondingly, daily-averaged horizontal advection of SSS reached the maximum on this day, with an advection rate of roughly 1.81×10^{-6} psu s^{-1}. After the Lekima passage, the surface currents gradually weakened and shifted offshore (Fig. 2c, d). From August 5 to August 11, horizontal advection contributed to about 0.51 psu of SSS increase (Fig. 2e). Consequently, due to the strong SSS gradients, horizontal advection contributes to the sea surface salinification induced by Lekima in the radar-covered region of CRP.

In addition to horizontal advection, the strong winds of TCs are likely to trigger strong subsurface vertical mixing and vertical advection, bringing subsurface salty water into surface layers. Moreover, freshwater flux resulting from runoff, evaporation, and precipitation associated with Lekima may also influence the SSS. These complex processes can be well resolved in the three-dimensional numerical model developed by Wu et al. in 2011 based on the Estuarine, Coastal, and Ocean Model (ECOM-si) (ref. 50). This model has been used in studying dynamics in the CRP and its interaction with TCs[36,42,50–54] (see "Numerical model simulations" in Methods). The ocean response to Lekima in the YECS is simulated using the

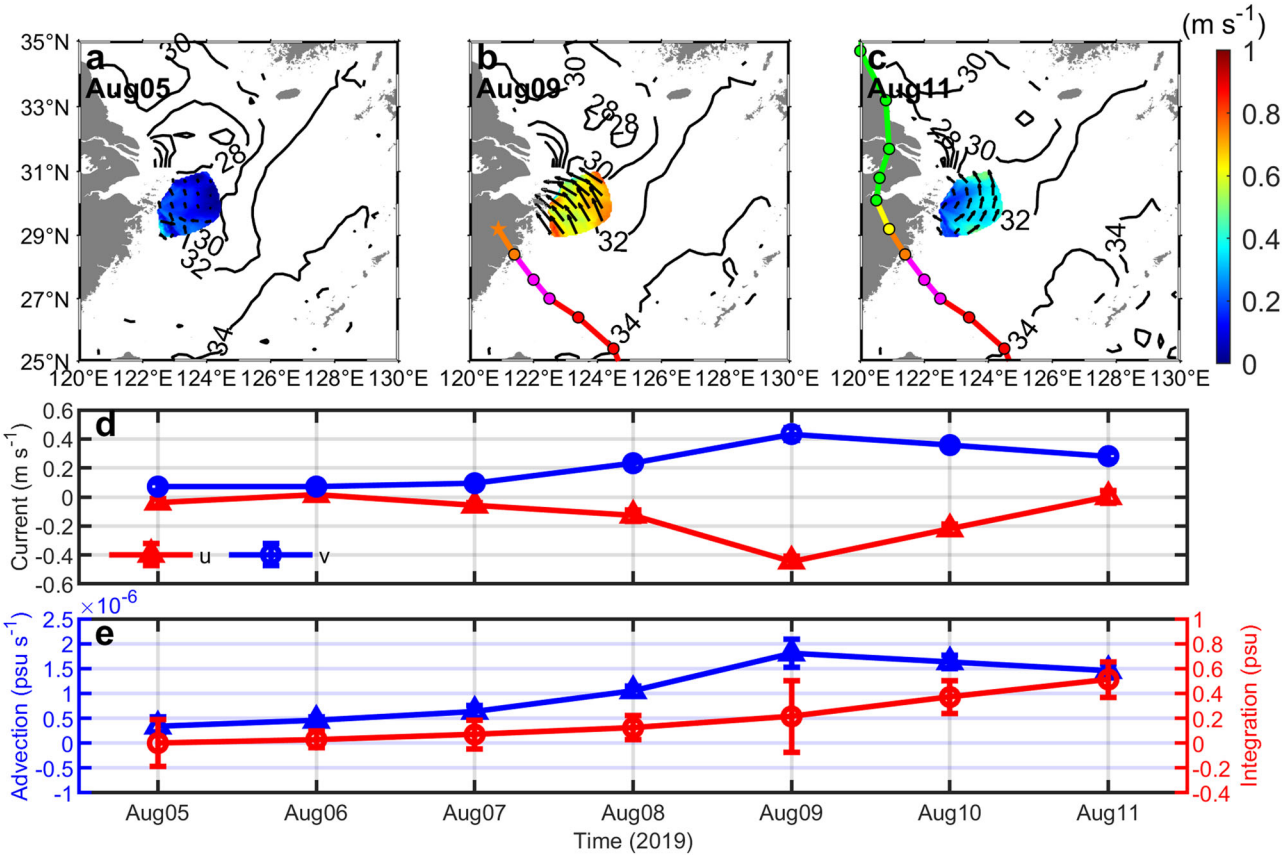

Fig. 2 | Sea surface salinity changes due to horizontal advection. a Radar-observed sea surface currents and satellite sea surface salinity on August 5 before the Lekima passage. Sea surface currents within the radar-covered region are represented by shaded colors and black arrows. Sea surface salinity contours are shown by black lines. **b–c** Same as (**a**), but for dates of August 9 and 11 during and after the Lekima passage, respectively. Colored-solid lines with dots denote the track of Lekima that has occurred. **d** Components of daily-mean sea surface currents on the x-axis (u, red line) and the y-axis (v, blue line). **e** Advection rate of salinity (blue line) and accumulated horizontal advection of salinity (red line). Error bars denote 95% confidence intervals.

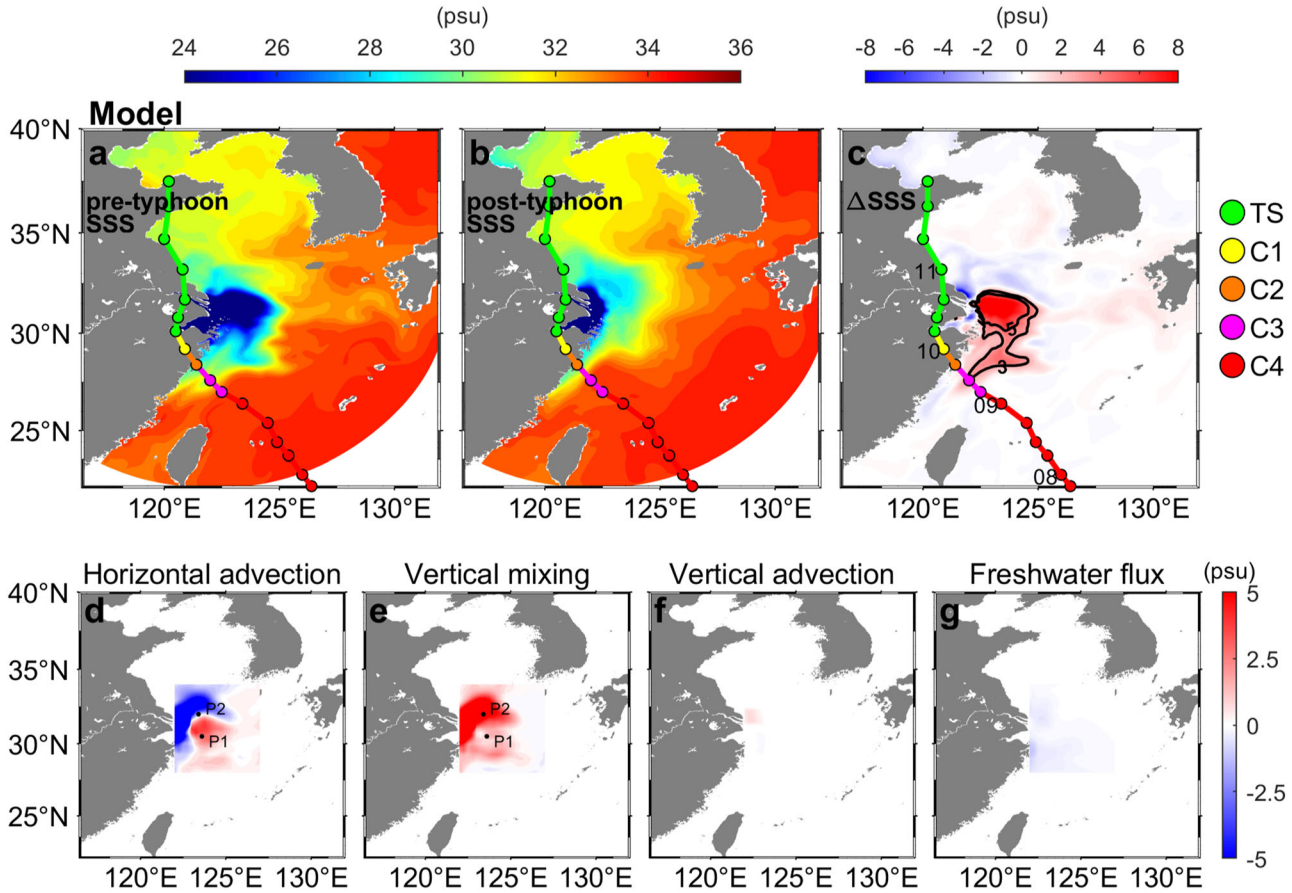

Fig. 3 | Model simulated sea surface salinity (SSS) responses to the Lekima passage and associated mixed-layer salinity budget analysis. a Spatial distribution of SSS before Lekima passage. The colored solid line with dots denotes the track of Lekima. **b** Same as (**a**), but for SSS after Lekima passage. **c** Same as (**a**), but for SSS changes induced by Lekima. The +3 and +5 psu isohalines are contoured. Contributions of horizontal advection (**d**), vertical mixing (**e**), vertical advection (**f**), and freshwater flux (**g**) to the sea surface salinification of Changjiang River Plume. The contributions are integrated from August 5 to 15. Black dots are referred to as P1 and P2, respectively. Abbreviations: TS tropical storm, C1 Category 1, C2 Category 2, C3 Category 3, C4 Category 4.

model. As shown in Fig. 3a–c, model simulations well reproduce satellite-observed pre-, post-Lekima SSS, and Lekima-induced sea surface salinification.

To comprehensively explore the mechanisms of the CRP sea surface salinification induced by Lekima, we conduct a mixed-layer salinity budget analysis (see "Mixed-layer salinity budget analysis" in Methods). Repeating calculations within the radar-covered region using the model output, horizontal advection contributed ~0.7 psu to the SSS increase, close to the observational estimate. In the whole CRP, horizontal advection and vertical mixing are both important factors controlling the sea surface salinification, while vertical advection and freshwater flux make slight contributions, averaging 0.02 psu and −0.18 psu, respectively (Fig. 3d–g). The slight contribution of vertical advection suggests that Lekima-induced upwelling did not reach the CRP sea surface salinification region. This is because upwelling typically occurs mostly around TC centers, which, in this case, were located inland and at a considerable distance to the south and west of the CRP (Supplementary Figs. 4 and 5) (see "Impact of upwelling" in Methods).

In the southeast CRP, both vertical mixing and horizontal advection contribute to the sea surface salinification. For example, at point P1 (30.5°N, 123.6°E), vertical mixing increases SSS by +1.4 psu, and horizontal advection increases SSS by +2.8 psu (Fig. 3d, e and Supplementary Fig. 6a–d). The positive contribution of vertical mixing and horizontal advection to sea surface salinification is due to subsurface salty waters being entrained into surface layers and southeast winds pushing surrounding salty waters to the CRP region, respectively. Nevertheless, in the northwest CRP from the Changjiang mouth to Jeju Island, while vertical mixing increases the SSS, horizontal advection decreases the SSS, counteracting the salinification effect induced by vertical mixing. For example, at point P2 (32.0°N, 123.4°E), vertical mixing contributes to an increase in SSS of +7.8 psu, while horizontal advection leads to a decrease of -1.3 psu (Fig. 3d, e and Supplementary Fig. 6e–g). The negative contribution of horizontal advection in this area is due to the southeast winds associated with Lekima generating northwestward ocean surface currents, which transport the extremely low salinity waters of the main CRP northwestward. The results indicate that horizontal advection can either enhance or counteract the sea surface salinification, depending on the directions of local horizontal SSS gradients and surface currents; in contrast, vertical mixing, which entrains saline water from the subsurface to the surface, consistently increases SSS in the CRP.

For individual TC cases with different attributes, including tracks, intensity, translation speed, and size, the mechanisms controlling sea surface salinification induced by TCs may be different in specific regions of CRP. For instance, along the Zhejiang and Fujian coasts, horizontal advection is the predominant process over vertical mixing during the passage of Bavi (2020), likely due to the presence of coastal currents[55]; in contrast, far from the coasts, vertical mixing is the dominant process over horizontal advection[20]. Additionally, although the CRP is shallow waters, the waters are not mixed to the bottom sea by Lekima, consistent with the finding in ref. 44 (see "Impact of shallow water" in Methods). Nevertheless, for strong and slow-moving TCs directly passing over the CRP and exerting strong wind stress, both shallow water effects and upwelling would be expected to occur and thus impact the sea surface salinification[6,20].

Potential role of TCs in restricting low-salinity water extension

As one of the most favorable fishing areas worldwide[39], the YECS in summertime is often threatened by an extremely low-salinity environment due to the CRP extension, which can cause massive mortality of marine life. For instance, owing to the low-salinity stress, unprecedented massive mortality of commercially important microbenthic animals occurred around Jeju Island in 1996 (ref. 37). Thus, SSS evolution and CRP extension have an important ecological impact on the YECS. Annually, influenced by the rapidly increasing discharge from the Changjiang River and the summer monsoon winds, the CRP extends offshore toward Jeju Island in a tongue-shaped pattern, reaching the minimum SSS in July and August (Supplementary Fig. 7). During these months, the full development of the CRP often coincides with the typical trajectory of TCs traversing the YECS. Analysis of Super Typhoon Lekima demonstrates that satellite observations successfully captured the spatiotemporal evolution of SSS under the influence of such TCs, highlighting the notable increase in SSS across the CRP region and an 83% contraction of low-salinity CRP due to TC-induced vertical mixing and horizontal advection.

From 2015 to 2022, 30 TCs passed through the CRP region, with 19 TCs occurring in July and August (Fig. 4a). Spatial patterns of SSS response to three TCs with typical tracks when passing over the CRP are shown in Fig. 4b–d. Regardless of these TCs occurring in the middle-, left-, or right side of the CRP region, all caused a widespread increase in SSS (encompassed by +1 psu isohaline) and thus CRP contraction. The surface salinification induced by all the TCs is further investigated based on satellite observations and model simulations. Figure 4e shows the temporal evolution of SSS averaged within the CRP region, illustrating that TCs pass over the CRP nearly every year (except 2016) and cause substantial SSS increases.

Noteworthy is the lower SSS events in 2016 and 2020 than in other years (Fig. 4e). In 2020, a record-breaking rainfall within the Changjiang River watershed led to an exceptional river discharge[56], likely explaining the extremely low SSS despite the three TCs' mitigating effects to some degree. Nevertheless, rainfall in 2016 was moderate, which is not a reasonable reason for the even lower SSS than in 2020. Coincidentally, no TCs passed over the CRP region in July and August 2016. If TCs were passing over, the extension of extremely low-SSS water should have been mitigated by TC-induced SSS increase. The co-occurrence of extremely low-SSS water and the absence of TCs in 2016 is not unique, as it also occurred in August 1996 (Supplementary Fig. 7). The extension of extremely low-SSS water in these years has resulted in severe ecological disasters[37,48,57].

The intermittent increases in SSS induced by TCs are merged in the seasonal cycle of CRP SSS, attributed to the seasonal Changjiang River discharge. To demonstrate the specific impact of TCs on the SSS changes, we conduct numerical experiments with or without TCs using the numerical model for July and August 2015–2022 (see "Numerical model simulations" in Methods). In the simulations with TCs, SSS changes are generally consistent with those observed by satellites. However, in simulations when TCs did not pass over the CRP during July and August, the simulated SSS is lower than those with TCs, with the maximum SSS decrease in 2015 and from 2017 to 2022 being −2.9, −0.8, −1.9, −2.9, −2.5, −1.8, and −1.1 psu, respectively (Fig. 4f).

Additionally, how SSS changes induced by TCs depend on TC attributes, including number, intensity, and translation speed, are explored (see "Numerical model simulations" in Methods). In July and August of 2019, two TCs, Danas (201906) and Lekima (201909), sequentially passed over the CRP region (Supplementary Fig. 8). Contrary to the contraction of the CRP from 125°E to the coastline by Lekima, in the absence of Lekima's passage, the low-salinity CRP waters would spread more extensively from 125°E to 127°E in the YECS (Supplementary Fig. 9). The average SSS from August 5 to 31 was 1.4 psu lower and the maximum SSS was 2.3 psu lower than conditions with Lekima. In contrast, when Danas were more intense or slower, the average SSS was larger in July and August (Supplementary Fig. 8). The findings suggest that recurring TCs, especially with high intensity and slow translation speed, play a crucial sustaining role for marine life in the YECS by alleviating the extension of extremely low-salinity CRP.

Discussion

During the boreal summer, the low-SSS CRP formed by Changjiang River discharge extends widely within the YECS, posing possible adverse effects such as mass mortalities of marine fish[40,46]. Meanwhile, TCs frequently pass over the CRP region, while how they moderate SSS changes and the associated mechanisms have been less explored. In this study, combining satellite and in-situ observations with modeling experiments, we characterize the SSS response to Super Typhoon Lekima (2019) and explore the associated mechanisms. Satellite SSS observations have an average bias and RMSE of only 0.09 psu and 0.16 psu, suggesting their reliability in capturing the SSS changes induced by Super Typhoon Lekima. We find that Lekima induced a widespread increase in SSS within the YECS, with the most profound increase observed within the CRP. The maximum SSS increase reaches 6.5 psu, and the low-SSS CRP, previously widely extending in the YECS, retreats to the Changjiang estuary with a contraction of 83%. This dramatic increase in SSS is primarily attributed to Lekima-induced vertical mixing and horizontal advection. Horizontal advection can either enhance or counteract the sea surface salinification, depending on the directions of local horizontal SSS gradients and surface currents; in contrast, vertical mixing, which entrains saline water from the subsurface to the surface, consistently increases SSS in the CRP. Vertical advection and freshwater flux contribute positively and negatively, but both slightly to the increase in SSS in the case of Lekima.

Considering that approximately three TCs pass over the developing CRP annually, the potential impact of TCs on the extension of low-salinity CRP is explored based on satellite observations and model experiments from 2015 to 2022. It is found that TC-induced SSS increase restricts extremely low-salinity water within the CRP, being of potential ecological significance in the YECS. Combining the impact of TCs on SSS with fishery recruitment or harvest records is an important area for further study. Additionally, as the haline stratification below low-SSS water can be favorable for the formation of extreme surface warming events such as marine heatwaves[20,48], TCs passing over the low-SSS water may be strengthened. Given that aquaculture and fisheries contribute an increasing share of nutrition for the global population, the oceanic salinity and temperature environment in the YECS is crucial for the local fishery, as it is one of the most favorable fishing areas worldwide. Our findings suggest the complex interplay between weather phenomena and marine ecological balance, underscoring the importance of monitoring these dynamic processes and enhancing their representation in numerical models for improving TC intensity forecasting and sustaining marine resources in the YECS.

Methods

Super Typhoon Lekima

Information on Lekima (2019), including its 6-hourly center location and 1-min sustained maximum winds distributed by the U. S. Joint Typhoon Warning Center (JTWC), is obtained from the International Best Track Archive for Climate Stewardship version 4.0 dataset[58]. Lekima, the most devastating typhoon in the 2019 Pacific typhoon season, developed as a tropical depression in the western tropical Pacific on August 4. After genesis, Lekima moved northwest and quickly strengthened to its lifetime peak intensity (~69 m s^{-1}) on August 8, equivalent to a Category 4 hurricane on the Saffir-Simpson Hurricane Scale. It weakened and made landfall in Zhejiang, China, with an intensity of approximately 46 m s^{-1} at 18 UTC on August 9. Then it moved northwards and traversed the Shandong Peninsula before disappearing on August 11. Overall, Lekima mainly influenced the YECS from August 9 to August 11. In addition, TC best track data from 2015 to 2022 are also used to investigate their effect on surface salinification over the CRP.

Satellite data

The satellite Soil Moisture Active Passive (SMAP) SSS L3 product (version 5.0), provided by the Remote Sensing Systems (RSS) since April 2015, is employed to examine the CRP SSS response to Super Typhoon Lekima. This dataset provides daily SSS based on the SSS average spanning an eight-day moving time window. We use SSS smoothed to approximately 70 km

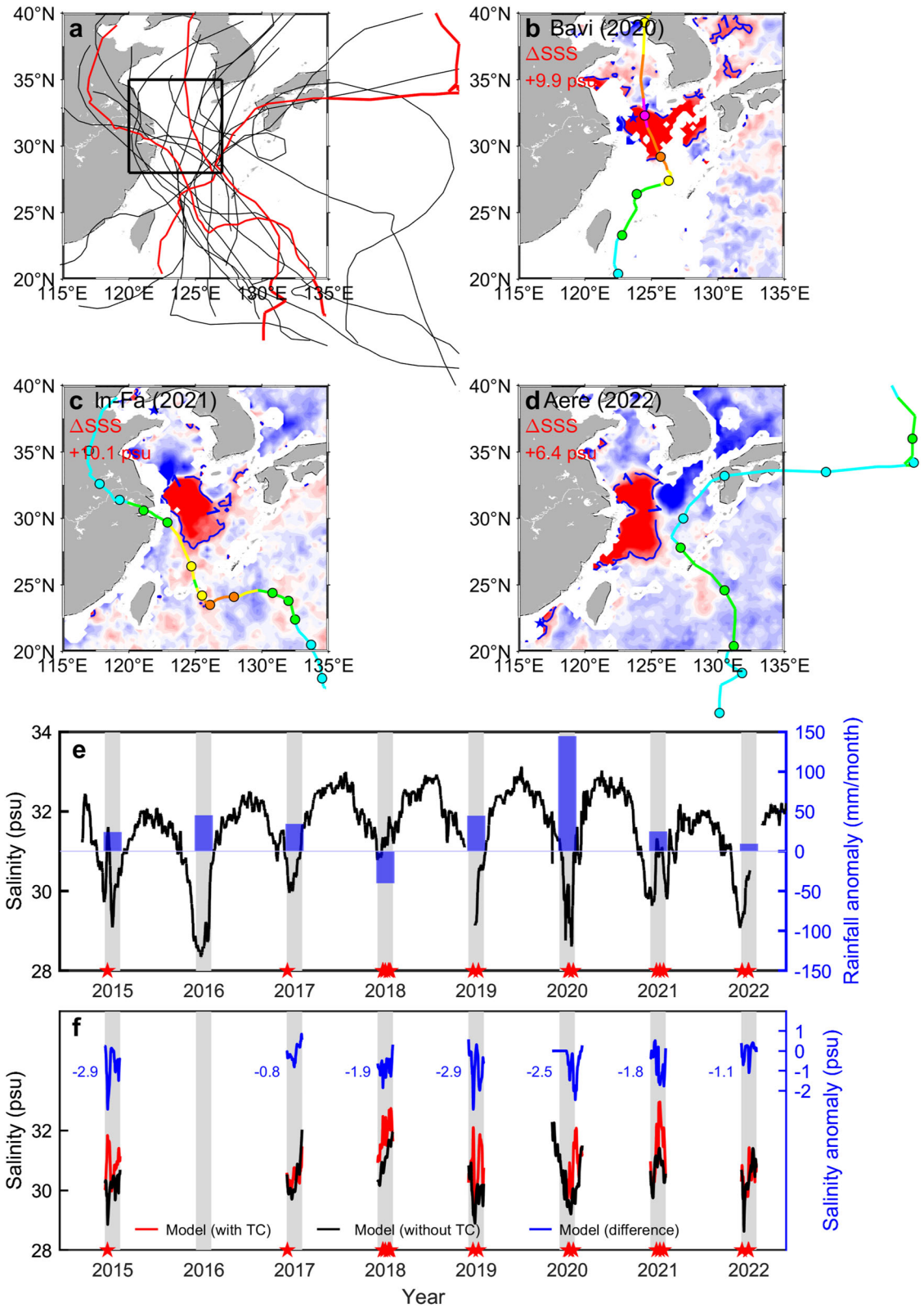

Fig. 4 | Impact of tropical cyclones on the sea surface salinification of Changjiang River Plume. a Tropical cyclone tracks that influenced the Changjiang River Plume region (represented by a black box) in July and August from 2015 to 2022. The box range is 28°N–35°N and 120°E–127°E. **b**–**d** Spatial patterns of SSS increase induced by three representative tropical cyclones. Solid lines with dots denote tropical cyclone tracks. +1 psu contours are presented, and the maximum value of the SSS increase is labeled on the top-left corner of each panel. **e** Time series of averaged sea surface salinity (SSS) in the Changjiang River Plume from satellite data. Shaded gray areas denote July and August of each year. Red stars on the x-axis denote tropical cyclones influencing the Changjiang River Plume region in July and August. Blue bars denote rainfall anomalies over the Changjiang River valley. **f** Simulated SSS in July and August each year with (red line) and without tropical cyclones (black line), and SSS difference between model experiments without and with tropical cyclones (blue line). The maximum SSS differences are labeled. Note that no simulated SSS and its differences are shown in 2016 since no tropical cyclones passed.

resolution (ref. 59). In situ SSS observations from a pre-Lekima deployed surface buoy B111 in the YECS are used to assess the accuracy of SMAP SSS data. The salinity sensor of B6001 is broken and thus has no SSS data available. Microwave and infrared merged OI SST with 9 km and daily resolution, provided by the RSS, is also employed to study the SST response[60]. Monthly rainfall data from the Climate Prediction Center Merged Analysis of Precipitation[61] are used to calculate the rainfall anomalies over the Changjiang River valley[56].

Radar observations

Contributions of horizontal advection to the SSS increase are estimated by combining satellite SSS and radar sea surface current observations. Although current data during TC conditions are difficult to observe[62], we obtained the data during Lekima from a high-frequency ground-wave radar installed at the coast. The radar transmits at a frequency of about 12 MHz and provides sea surface current maps every 10 min with a high horizontal resolution of $0.05' \times 0.05'$. Sea surface currents are measured through the Doppler shift of the radio waves, which are backscattered by the ocean surface waves. After filtering out tidal signals, daily-averaged currents are used. The domain of radar observation reaches up to $3.2 \times 10^4 \mathrm{km}^2$ in the YECS, covering most of the CRP extension area in the summer.

Numerical model simulations

To explore mechanisms of the CRP sea surface salinification induced by Lekima and the dependences of SSS changes on TC attributes, we conduct numerical experiments with the model developed by Wu et al. in 2011 (ref. 50.). The model was configured based on the 3D Estuarine, Coastal, and Ocean Model (ECOM-si) that was improved by Wu and Zhu in 2010 with a new advection scheme[63].

The model domain covers the Bohai Sea, Yellow Sea, East China Sea, and parts of the northwestern Pacific Ocean. Model grid comprises 367 by 319 cells horizontally, with resolution ranging from several hundred meters near the river mouth to 2–3 km in regions where the main body of the plume expands. Vertically, the model consisted of 20 non-uniform sigma layers, with refinement near the surface.

Boundary and initial conditions for salinity and temperature are from the Simple Ocean Data Assimilation dataset. Hydrodynamic open ocean boundary conditions are driven by velocity, incorporating both shelf and tidal currents. Changjiang River discharge data are from the Changjiang Sediment Bulletin (http://www.cjh.com.cn/). Air–sea heat flux, including solar radiation, atmospheric radiation, sensible heat flux, and latent heat flux, was calculated with a bulk formula[64] based on simulated sea surface temperature, 2-m temperature, mean sea level pressure, 10-m wind speed, 2-m relative humidity, and total cloud cover sourced from ERA5 hourly data of ECMWF. Air–sea freshwater flux (i.e., evaporation minus precipitation, EMP) was also prescribed in the model based on data from ERA5. More details on the numerical model setup can be found in ref. 50.

Using this model, we conduct numerical simulations with or without TCs, which allow us to isolate and demonstrate the specific impact of TCs on CRP SSS. These simulations are carried out for July and August each year from 2015 to 2022. For the experimental runs without TCs, we remove the atmospheric fields during TCs and replace them with linear interpolations of their neighbors before and after TCs. Wind observations from buoys B111 and B6001 support the accuracy of ERA5 wind direction data (Supplementary Fig. 3). Nevertheless, considering that wind data from ERA5 exhibit smaller bias in strong TCs, we utilize the Jelesnianski model[65] to construct wind fields for TCs as inputs for the numerical experiments with TCs, to accurately simulate the oceanic response to TCs. Winds and pressure based on the Jelesnianski model are calculated:

$$V = \begin{cases} \frac{r}{R_{\max}+r}\left(V_{\mathrm{ox}}\mathbf{i} + V_{\mathrm{oy}}\mathbf{j}\right) + V_{\max}\left(\frac{r}{R_{\max}}\right)^{\frac{3}{2}}\frac{1}{r}\left(A\mathbf{i} + B\mathbf{j}\right)\left(r \le R_{\max}\right) \\ \frac{R_{\max}}{R_{\max}+r}\left(V_{\mathrm{ox}}\mathbf{i} + V_{\mathrm{oy}}\mathbf{j}\right) + V_{\max}\left(\frac{R_{\max}}{r}\right)^{\frac{1}{2}}\frac{1}{r}\left(A\mathbf{i} + B\mathbf{j}\right)\left(r > R_{\max}\right) \end{cases} \quad (1)$$

$$P_a = \begin{cases} P_c + \frac{1}{4}\left(P_n - P_c\right)\left(\frac{r}{R_{\max}}\right)^3 \left(r \le R_{\max}\right) \\ P_n - \frac{3}{4}\left(P_n - P_c\right)\left(\frac{R_{\max}}{r}\right) \left(r > R_{\max}\right) \end{cases} \quad (2)$$

$$A = -\left[\left(x - x_c\right)\sin\theta + \left(y - y_c\right)\cos\theta\right] \quad (3)$$

$$B = \left[\left(x - x_c\right)\cos\theta - \left(y - y_c\right)\sin\theta\right] \quad (4)$$

$$V_{\max} = 3.029\left(P_n - P_c\right)^{0.664} \quad (5)$$

$$R_{\max} = 28.52\ \tanh\left[0.0873(\varphi - 28) + 12.22\mathrm{e}^{\frac{P_c - P_n}{33.86}} + 0.2V_{\mathrm{mov}} + M\right] \quad (6)$$

where x and y denote locations of wind to be calculated (referred to as calculated points), x_c and y_c denote locations of TC centers, r denotes distances from calculated points to TC centers, V denotes winds at calculated points, V_{ox} and V_{oy} denote wind projected to x and y direction, respectively, i and j are unit vectors of the x and y coordinate axis, V_{max} denotes the maximum winds of TCs, R_{max} denotes radius of the maximum TC winds, P_a denotes pressure at calculated points, P_c and P_n denote the minimum pressure at TC centers and atmosphere pressure at infinity, respectively, φ denotes latitude of TC centers, V_{mov} denotes translation speed of TCs, θ denotes inflow angle, using 20°, and M denotes starting radius, using 25 km.

To better simulate wind fields far from TC centers, we use composited winds from model winds and background ERA5 winds. The composited winds are calculated:

$$V_{\mathrm{com}} = (1 - \alpha)V + \alpha V_b \quad (7)$$

$$\alpha = \frac{c^4}{1 + c^4} \quad (8)$$

$$c = \frac{r}{nR_{\max}} \quad (9)$$

where V_{com} denotes the composite winds, V denotes model winds, V_b denotes background ERA5 winds, α denotes a weighting coefficient, and n is set to 5 here.

To analyze the dependence of CRP SSS changes on TC attributes, including TC number, intensity, and translation speed, we further conduct three additional numerical experiments. In July and August of 2019, two TCs, Danas (201906) and Lekima (201909), passed over the CRP region. To examine the impact of TC frequency on SSS, we conduct an experiment where we retained Danas but removed Lekima from the model. To explore the impact of TC intensity on SSS, we increase the maximum intensity of Danas by 30 m s^{-1}. Lastly, to explore the impact of the translation speed of TCs on SSS, we reduce the translation speed of Danas by 50%.

Mixed-layer salinity budget analysis

To explore mechanisms for CRP sea surface salinification, we conduct a mixed-layer salinity budget analysis. The mixed layer salinity evolution equation[66] is:

$$\frac{\partial S}{\partial t} = -\vec{u}\cdot\overrightarrow{\nabla_h}S - \vec{w}\cdot\overrightarrow{\nabla_z}S - \frac{1}{h}\frac{\partial h}{\partial t}\left(S - S_{z=h}\right) + \frac{1}{h}\left(\kappa\frac{\partial S}{\partial z}\right)_{z=h} + \frac{(E - P - R)S}{h} + \varepsilon \quad (10)$$

where S is mixed-layer-average salinity, t is time, u and w are horizontal and vertical ocean currents, h is mixed-layer depth which is calculated using a criterion of a 0.125 kg m^{-3} density change relative to near-surface value, κ is the vertical diffusion coefficient, E is evaporation, P is precipitation, R is river runoff, and ε is error including horizontal diffusion, which can be neglected.

Right-hand terms 1 and 2 in Eq. (10) denote the horizontal advection and vertical advection, respectively; terms 3 and 4 denote the vertical mixing, and term 5 denote the freshwater flux.

Impact of upwelling

Based on the model simulations, we examine the impact of upwelling on Lekima-induced CRP sea surface salinification. Theoretically, the upwelling, resulting from Ekman pumping associated with positive wind stress curl of TCs, occurs mostly around TC centers. On August 9 and 10, Lekima reached its weakening stage, moving northwestward to the China mainland, and making landfall in Zhejiang. Therefore, Lekima exerted relatively weak maximum winds in the CRP (~20 m s^{-1}) and no positive wind stress curl because its track was south and west of the CRP. When examining the evolution of salinity and temperature (S/T) profiles at a point (27.6°N, 122°E, as indicated by a red star in Supplementary Fig. 4a) directly beneath Lekima center at 1200 UTC on August 9 before landfall, we indeed find an upwelling signal occurred following TC passage (Supplementary Fig. 4b, c). This upwelling led to a maximum uplift of 22 m in isohalines and isotherms, thereby enhancing sea surface salinification and cooling.

However, an upwelling signal at station (123.6°E, 30.2°N) within the CRP, which is about 280 km away from Lekima center, is very weak (Supplementary Fig. 4g–i). Moreover, due to the presence of topography, the onshore winds during Lekima's passage seem to cause a downwelling in the coastal waters. This is supported by a recent study[55], which identified that Bavi (2020) also induced a downwelling in the coastal waters. Additionally, weak tidal signals can also be seen in the isohalines and isotherms. This indicates that the Lekima-induced upwelling may not extend to the main low-salinity CRP region.

To demonstrate whether the Lekima-induced upwelling extended to the CRP, we explore the extended range of the Lekima-induced upwelling by examining a cross-track T/S section from 121.6°E (27.1°N) to 122.5°E (28.0°N), as indicated by the green line in Supplementary Fig. 4d. Before Lekima passage, horizontal gradients of T/S and water depth along the selected cross-track section are minimal. After Lekima, strong upwelling emerged around regions beneath the Lekima center, however, the upwelling extends northeastward no more than (122.3°E, 27.8°N), far away from the CRP region (Supplementary Fig. 4e, f). Further, by examining salinity and temperature profiles for each point in the CRP sea surface salinification region, we find that no point was marked with upwelling. Therefore, during the passage of Lekima near the CRP with its center located southward, westward, or inland, the upwelling cannot reach the low-salinity CRP region and thus cannot contribute to the sea surface salinification.

Theoretically, if no land existed when Lekima was westward of the CRP on August 10, Lekima would induce upwelling beneath its center. We examine the potential upwelling by conducting a three-dimensional Price-Weller-Pinkel (3DPWP) model experiment[67]. Since Lekima did make landfall, pre-Lekima T/S profiles beneath Lekima's center are unavailable. Thus, we use T/S profiles from the location (125°E, 26.5°N) in the CRP instead, sourced from the World Ocean Atlas 2018 (WOA18), as input for the 3DPWP model. After Lekima, by examining the simulated T/S section from 114°E to 127°E (30.6°N), we find that upwelling occurs approximately 200 km within the Lekima center (Supplementary Fig. 5). In reality, the area where upwelling occurs is mostly inland and cannot reach the main CRP regions that we focus on.

Impact of shallow water

When a strong and/or slow-moving TC passes over the YECS, exerting high stress on the ocean, the shallow waters over the CRP region are likely to become totally mixed from surface to bottom. In such scenarios, the shallow waters restrict vertical mixing, thereby potentially limiting the sea surface's salinity and temperature response to the TC.

Previous studies[44] indicate that mixing depth can extend to the bottom of the Yellow Sea under TC winds of approximately 35 m s^{-1} (with a translation speed of 6 m s^{-1}). In the case of Lekima, it made landfall when passing near the CRP and exhibited relatively weak wind speeds (~20 m s^{-1}). Moreover, barrier layers created by Changjiang diluted water are likely to resist Lekima-induced vertical mixing[20]. Consequently, in the main CRP sea surface salinification region, the mixing did not affect the entire water column.

Moreover, we conduct experiments to examine whether shallow waters in the main CRP restrict the extent of sea surface salinification. This examination utilized the 1DPWP model to compare the magnitudes of salinification between shallow water and open ocean conditions[20]. The 1DPWP model is a "shear instability" model that applies the atmospheric forcing to initial vertical profiles of temperature, salinity, and currents and calculates their time evolution. It presumes that when the bulk Richardson number is less than 0.65 or the gradient Richardson number falls below 0.25, vertical mixing is initiated. Wind stress is calculated based on the bulk formula[68]. Precipitation data are obtained from ERA5. Pre-TC salinity and temperature profiles are based on monthly profiles for August from the WOA18 dataset. Pre-TC currents are set to zero. These profiles are interpolated to a vertical resolution of 1 m within the 1DPWP model. The model is configured with a time step increment of 300 s, and data is saved to the output file every hour.

In shallow water conditions, we use original salinity and temperature profiles from the WOA18. For open ocean conditions, we extend these profiles to a depth of 1500 m: within the true shallow water depth, the extension is based on the original profiles; for depths beyond the true bottom water depth, the extension is based on profiles from the open ocean at equivalent latitudes in the Western North Pacific, adjusting for an offset at the true bottom shallow water depth. The simulations revealed a marginal difference of 0.02 psu between the shallow water and open ocean conditions, indicating that shallow waters have a negligible impact on the vertical mixing and sea surface salinification induced by Lekima.

Data availability

The data used in this study are available at https://doi.org/10.6084/m9.figshare.28784516. Best track data are available at the International Best Track Archive for Climate Stewardship at https://climatedataguide.ucar.edu/climate-data/ibtracs-tropical-cyclone-best-track-data. SMAP salinity and MW_IR temperature products are available at Remote Sensing Systems at https://www.remss.com. Monthly precipitation data are obtained from the Climate Prediction Center Merged Analysis of Precipitation at https://climatedataguide.ucar.edu/climate-data/cmap-CRPc-merged-analysis-precipitation. European Center for Medium-Range Weather Forecasts Reanalysis v5 dataset at https://www.ecmwf.int/en/forecasts/dataset/ecmwf-reanalysis-v5. World Ocean Atlas 2018 is available at https://www.ncei.noaa.gov/products/world-ocean-atlas. Simple Ocean Data Assimilation data are available at https://www2.atmos.umd.edu/~ocean/. Changjiang Sediment Bulletin is available at http://www.cjh.com.cn/.

Received: 22 August 2024; Accepted: 21 April 2025;
Published online: 02 May 2025

References

1. Emanuel, K. Tropical cyclones. *Annu. Rev. Earth Planet. Sci.* **31**, 75–104 (2003).
2. Price, J. F. Upper ocean response to a hurricane. *J. Phys. Oceanogr.* **11**, 153–175 (1981).
3. Lin, I. I., Liu, W. T., Wu, C. C., Chiang, J. C. H. & Sui, C. H. Satellite observations of modulation of surface winds by typhoon-induced upper ocean cooling. *Geophys. Res. Lett.* **30**, 1131 (2003).
4. Yang, D., Yin, B., Liu, Z. & Feng, X. Numerical study of the ocean circulation on the East China Sea shelf and a Kuroshio bottom branch northeast of Taiwan in summer. *J. Geophys. Res. Oceans* **116**, C05015 (2011).
5. Reul, N. et al. Satellite observations of the sea surface salinity response to tropical cyclones. *Geophys. Res. Lett.* **48**, e2020GL091478 (2021).
6. Li, Y. et al. Three types of typhoon-induced upwellings enhance coastal algal blooms: A case study. *J. Geophys. Res. Oceans* **127**, e2022JC018448 (2022).

7. Yablonsky, R. M. & Ginis, I. Limitation of one-dimensional ocean models for coupled hurricane–ocean model forecasts. *Mon. Weather Rev.* **137**, 4410–4419 (2009).
8. Fu, D. et al. Impact of two typhoons on the marine environment in the Yellow Sea and East China Sea. *Chin. J. Ocean. Limnol.* **34**, 871–884 (2016).
9. Podeti, S. R., Viswanadhapalli, Y., Nellipudi, N. R., Rao, S. R. & Ramakrishna, S. S. V. S. Impact of ocean–atmosphere coupling on the simulation of a monsoon depression over the bay of Bengal. *Pure Appl. Geophys.* **179**, 1–24 (2022).
10. Balaguru, K. et al. Ocean barrier layers' effect on tropical cyclone intensification. *Proc. Natl. Acad. Sci. USA* **109**, 14343–14347 (2012).
11. Ito, K., Kuroda, T., Saito, K. & Wada, A. Forecasting a large number of tropical cyclone intensities around Japan using a high-resolution atmosphere–ocean coupled model. *Weather Forecast.* **30**, 793–808 (2015).
12. Da, N. D., Foltz, G. R. & Balaguru, K. Observed global increases in tropical cyclone-induced ocean cooling and primary production. *Geophys. Res. Lett.* **48**, e2021GL092574 (2021).
13. Cione, J. J. & Uhlhorn, E. W. Sea surface temperature variability in hurricanes: Implications with respect to intensity change. *Mon. Wea. Rev.* **131**, 1783–1796 (2003).
14. Zheng, Z.-W., Ho, C.-R. & Kuo, N.-J. Importance of pre-existing oceanic conditions to upper ocean response induced by Super Typhoon Hai-Tang. *Geophys. Res. Lett.* **35**, L20603 (2008).
15. Lloyd, I. D. & Vecchi, G. A. Observational evidence for oceanic controls on hurricane intensity. *J. Clim.* **24**, 1138–1153 (2011).
16. Mei, W. & Pasquero, C. Spatial and temporal characterization of sea surface temperature response to tropical cyclones. *J. Clim.* **26**, 3745–3765 (2013).
17. Guan, S., Zhao, W., Huthnance, J., Tian, J. & Wang, J. Observed upper ocean response to typhoon Megi (2010) in the Northern South China Sea. *J. Geophys. Res. Oceans* **119**, 3134–3157 (2014).
18. Wang, G., Wu, L., Johnson, N. C. & Ling, Z. Observed three-dimensional structure of ocean cooling induced by Pacific tropical cyclones. *Geophys. Res. Lett.* **43**, 7632–7638 (2016).
19. Liu, Y. et al. Effect of storm size on sea surface cooling and tropical cyclone intensification in the western North Pacific. *J. Clim.* **36**, 7277–7296 (2023).
20. Pun, I. F., Hsu, H. H., Moon, I. J., Lin, I. I. & Jeong, J. Y. Marine heatwave as a supercharger for the strongest typhoon in the East China Sea. *npj Clim. Atmos. Sci.* **6**, 128 (2023).
21. Domingues, R. et al. Upper ocean response to Hurricane Gonzalo (2014): Salinity effects revealed by targeted and sustained underwater glider observations. *Geophys. Res. Lett.* **42**, 7131–7138 (2015).
22. Steffen, J. & Bourassa, M. Barrier Layer Development Local to Tropical Cyclones based on Argo Float Observations. *J. Phys. Oceanogr.* **48**, 1951–1968 (2018).
23. Yue, X. et al. Upper ocean response to typhoon Kalmaegi and Sarika in the South China sea from Multiple-satellite observations and numerical simulations. *Remote Sens* **10**, 348 (2018).
24. Chaudhuri, D., Sengupta, D., D'Asaro, E., Venkatesan, R. & Ravichandran, M. Response of the salinity-stratified Bay of Bengal to cyclone Phailin. *J. Phys. Oceanogr.* **49**, 1121–1140 (2019).
25. Sanford, T. B., Price, J. F., Girton, J. B. & Webb, D. C. Highly resolved observations and simulations of the ocean response to a hurricane. *Geophys. Res. Lett.* **34**, L13604 (2007).
26. Hlywiak, J. & Nolan, D. S. The influence of oceanic barrier layers on tropical cyclone intensity as determined through idealized, coupled numerical simulations. *J. Phys. Oceanogr.* **49**, 1723–1745 (2019).
27. Dzwonkowski, B. et al. Cascading weather events amplify the coastal thermal conditions prior to the shelf transit of Hurricane Sally (2020). *J. Geophys. Res. Oceans* **126**, e2021JC017957 (2021).
28. Chacko, N. Insights into the haline variability induced by cyclone Vardah in the Bay of Bengal using SMAP salinity observations. *Remote Sens. Lett.* **9**, 1205–1213 (2018).
29. Reul, N. et al. Multisensor observations of the Amazon-Orinoco river plume interactions with hurricanes. *J. Geophys. Res. Oceans* **119**, 8271–8295 (2014).
30. Sun, J., Vecchi, G. & Soden, B. Sea surface salinity response to tropical cyclones based on satellite observations. *Remote Sens* **13**, 420 (2021).
31. Grodsky, S. A. et al. Haline hurricane wake in the Amazon/Orinoco plume: AQUARIUS/SACD and SMOS observations. *Geophys. Res. Lett.* **39**, L20603 (2012).
32. Balaguru, K. et al. Pronounced impact of salinity on rapidly intensifying tropical cyclones. *Bull. Am. Meteor. Soc.* **101**, E1497–E1511 (2020).
33. Lie, H. J., Cho, C. H., Lee, J. H. & Lee, S. Structure and eastward extension of the Changjiang River plume in the East China Sea. *J. Geophys. Res. Oceans* **108**, 3077 (2003).
34. Moon, J. H., Hirose, N., Pang, I. C. & Hyun, K. H. Modeling offshore freshwater dispersal from the Changjiang River and controlling factors during summer. *Terr. Atmos. Ocean. Sci.* **23**, 247–260 (2012).
35. Moon, J. H., Pang, I. C. & Yoon, J. H. Response of the Changjiang diluted water around Jeju Island to external forcings: A modeling study of 2002 and 2006. *Cont. Shelf Res.* **29**, 1549–1564 (2009).
36. Wu, H., Shen, J., Zhu, J., Zhang, J. & Li, L. Characteristics of the Changjiang plume and its extension along the Jiangsu Coast. *Cont. Shelf Res.* **76**, 108–123 (2014).
37. Seo, H. L., Cho, Y. G., Seo, H. Y. & Kim, D. H. Mass mortality of macrobenthic animals around Jeju Island in 1996: Roles of physical factors. *Korean J. Environ. Biol.* **17**, 175–182 (1999).
38. Xu, M. et al. Seasonal distribution of the early life stages of the small yellow croaker (Larimichthys polyactis) and its dynamic controls adjacent to the Changjiang River Estuary. *Fish. Oceanogr.* **32**, 390–404 (2023).
39. Chen, H., Yu, Z., Yao, Q., Mi, T. & Liu, P. Nutrient concentrations and fluxes in the Changjiang Estuary during summer. *Acta Oceanol. Sin.* **29**, 107–119 (2010).
40. Lee, J. H. et al. Impact of typhoons on the Changjiang plume extension in the Yellow and East China Seas. *J. Geophys. Res. Oceans* **122**, 4962–4973 (2017).
41. Kil, B. & Kil, T. Sea surface salinity changes around the Jeju Island after Typhoon Chaba. *2017 IEEE Underwater Technology (UT)*, Busan, Korea (South), pp 1–2 (2017).
42. Zhang, Z., Wu, H., Yin, X. & Qiao, F. Dynamical response of Changjiang River plume to a severe typhoon with the surface wave-induced mixing. *J. Geophys. Res. Oceans* **123**, 9369–9388 (2018).
43. Wang, J. et al. Wave–current interaction by Typhoon Fongwong on saline water intrusion and vertical stratification in the Yangtze River Estuary. *Estuar., Coast. Shelf Sci.* **279**, 108138 (2022).
44. Guan, S. et al. Tropical cyclone-induced sea surface cooling over the Yellow Sea and Bohai Sea in the 2019 Pacific typhoon season. *J. Mar. Syst.* **217**, 103509 (2021).
45. Howes, N. C. et al. Hurricane-induced failure of low salinity wetlands. *Proc. Natl Acad. Sci. USA* **107**, 14014–14019 (2010).
46. Park, T., Jang, C. J., Jungclaus, J. H., Haak, H. & Park, W. Effects of the Changjiang river discharge on sea surface warming in the Yellow and East China Seas in summer. *Cont. Shelf Res.* **31**, 15–22 (2011).
47. Hong, J.-S. et al. Role of salinity-induced barrier layer in air-sea interaction during the intensification of a typhoon. *Front. Mar. Sci.* **9**, 844003 (2022).
48. Moon, J. H. et al. Contribution of low-salinity water to sea surface warming of the East China Sea in the summer of 2016. *Prog. Oceanogr.* **175**, 68–80 (2019).
49. Reul, N. et al. Overview of the first SMOS sea surface salinity products. Part I: quality assessment for the second half of 2010. *IEEE Trans. Geosci. Remote Sens.* **50**, 1636–1647 (2012).
50. Wu, H., Zhu, J., Shen, J. & Wang, H. Tidal modulation on the Changjiang River plume in summer. *J. Geophys. Res.* **116**, C08017 (2011).

51. Wu, H. Cross-shelf penetrating fronts: a response of buoyant coastal water to ambient pycnocline undulation. *J. Geophys. Res. Oceans* **120**, 5101–5119 (2015).
52. Yuan, R., Wu, H., Zhu, J. & Li, L. The response time of the Changjiang plume to river discharge in summer. *J. Mar. Syst.* **154**, 82–92 (2016).
53. Huang, M., Liang, X. S., Wu, H. & Wang, Y. Different generating mechanisms for the summer surface cold patches in the Yellow Sea. *Atmos. Ocean* **56**, 199–211 (2018).
54. Wu, T. & Wu, H. Tidal mixing sustains a bottom-trapped river plume and buoyant coastal current on an energetic continental shelf. *J. Geophys. Res. Oceans* **123**, 8026–8051 (2018).
55. Meng, Q. et al. Response process of coastal hypoxia to a passing typhoon in the East China Sea. *Front. Mar. Sci.* **9**, 892797 (2022).
56. Zhou, Z. Q., Xie, S. P. & Zhang, R. Historic Yangtze flooding of 2020 tied to extreme Indian Ocean conditions. *Proc. Natl Acad. Sci. USA* **118**, e2022255118 (2021).
57. Sun, Q. et al. Massive nutrients offshore transport off the Changjiang Estuary in flooding summer of 2020. *Front. Mar. Sci.* **10**, 1076336 (2023).
58. Knapp, K. R., Kruk, M. C., Levinson, D. H., Diamond, H. J. & Neumann, C. J. The international best track archive for climate stewardship (IBTrACS) unifying tropical cyclone data. *Bull. Am. Meteor. Soc.* **91**, 363–376 (2010).
59. Meissner, T. et al. Remote Sensing Systems SMAP Ocean Surface Salinities (Version 5.0) [Dataset]. Remote Sensing Systems, Santa Rosa, CA, USA. https://doi.org/10.5067/SMP50-3SPCS (2022).
60. Wentz, F. J., Gentemann, C., Smith, D. & Chelton, D. Satellite measurements of sea surface temperature through clouds. *Science* **288**, 847–850 (2000).
61. Xie, P. & Arkin, P. A. Analyses of global monthly precipitation using gauge observations, satellite estimates, and numerical model predictions. *J. Clim.* **9**, 840–858 (1996).
62. Lin, J. et al. Monitoring ocean currents during the passage of Typhoon Muifa using optical-fiber distributed acoustic sensing. *Nat. Commun.* **15**, 1111 (2024).
63. Wu, H. & Zhu, J. Advection scheme with 3rd high-order spatial interpolation at the middle temporal level and its application to saltwater intrusion in the Changjiang Estuary. *Ocean Model* **33**, 33–51 (2010).
64. Ahsan, A. K. M. Q. & Blumberg, A. F. Three-dimensional hydrothermal model of Onondaga Lake, New York. *J. Hydraul. Eng.* **125**, 912–923 (1999).
65. Li, A. et al. Modeling wave effects on storm surge from different typhoon intensities and sizes in the South China Sea. *Estuar. Coast. Shelf Sci.* **235**, 106551 (2020).
66. Chen, Y., Xiao, C., Zhang, Y. & Lai, Z. The mixed layer salinity budget in the Northern South China Sea: a modeling study. *J. Mar. Sci. Eng.* **11**, 1693 (2023).
67. Price, J. F., Weller, R. A. & Pinkel, R. Diurnal cycling: observations and models of the upper ocean response to diurnal heating, cooling, and wind mixing. *J. Geophys. Res.* **91**, 8411–8427 (1986).
68. Oey, L.-Y., Ezer, T., Wang, D.-P., Fan, S.-J. & Yin, X.-Q. Loop Current warming by Hurricane Wilma. *Geophys. Res. Lett.* **33**, L08613 (2006).

Acknowledgements

This study is supported by the National Key Research and Development Program (No. 2022YFC3104300), the National Natural Science Foundation of China (Nos. 42476029 and 42476001), the Innovation Program of Shanghai Municipal Education Commission (No. 2021-01-07-00-08-E00102), and the Fundamental Research Funds for the Central Universities (Nos. 202001013129 and 1901013184).

Author contributions

S.G. conceptualized the idea and designed the analysis. H.W. and W.Z. modified the idea. M.H., S.G., Z.W., and Y.Z. collected the data and performed the analysis. Y.L. and H.W. conducted the numerical simulation. C.L. and Z.L. provided the radar data. I.L., F.J., and W.Z. supervised the work. M.H. and Y.Z. drafted the paper, and S.G. and H.W. revised it. W.Z., W.W., X.H., C.L., Z.L., X.L., and J.T. provided comments and improved the paper. All authors discussed the results and approved the submitted version.

Competing interests

The authors declare no competing interests.

Additional information

Supplementary information The online version contains supplementary material available at https://doi.org/10.1038/s43247-025-02317-x.

Correspondence and requests for materials should be addressed to Shoude Guan, Hui Wu or Wei Zhao.

Peer review information *Communications Earth & Environment* thanks Nicolas Reul and Zhilong Liu for their contribution to the peer review of this work. Primary Handling Editors: José Luis Iriarte Machuca and Alireza Bahadori. A peer review file is available.